Downloaded from orbit.dtu.dk on: Dec 08, 2024

DTU Library

Radial Nanowire Light-Emitting Diodes in the $(Al_xGa_{1-x})yIn_{1-y}P$ Material System

Berg, Alexander; Yazdi, Sadegh; Nowzari, Ali; Storm, Kristian; Jain, Vishal; Vainorius, Neimantas; Samuelson, Lars ; Wagner, Jakob Birkedal; Borgström, Magnus T

Published in:
Nano Letters

Link to article, DOI:
10.1021/acs.nanolett.5b04401

Publication date:
2016

Document Version
Peer reviewed version

Link back to DTU Orbit

Citation (APA):
Berg, A., Yazdi, S., Nowzari, A., Storm, K., Jain, V., Vainorius, N., Samuelson, L., Wagner, J. B., & Borgström, M. T. (2016). Radial Nanowire Light-Emitting Diodes in the $(Al_xGa_{1-x})yIn_{1-y}P$ Material System. *Nano Letters*, *16*(1), 656-62. https://doi.org/10.1021/acs.nanolett.5b04401

General rights
Copyright and moral rights for the publications made accessible in the public portal are retained by the authors and/or other copyright owners and it is a condition of accessing publications that users recognise and abide by the legal requirements associated with these rights.

- Users may download and print one copy of any publication from the public portal for the purpose of private study or research.
- You may not further distribute the material or use it for any profit-making activity or commercial gain
- You may freely distribute the URL identifying the publication in the public portal

If you believe that this document breaches copyright please contact us providing details, and we will remove access to the work immediately and investigate your claim.

Radial nanowire light-emitting diodes in the $(Al_xGa_{1-x})_yIn_{1-y}P$ material system

Alexander Berg,[†] *Sadegh Yazdi,*[‡,⊥] *Ali Nowzari,*[†] *Kristian Storm,*[†] *Vishal Jain,*[†,§] *Neimantas Vainorius,*[†] *Lars Samuelson,*[†] *Jakob B. Wagner,*[‡] *Magnus T. Borgström*[†,*]

[†]Solid State Physics and NanoLund, Lund University, Box 118, SE-221 00, Lund, Sweden

[‡]Center for Electron Nanoscopy, Technical University of Denmark, DK 2800 Kgs. Lyngby, Denmark

[§]Laboratory of Mathematics, Physics and Electrical Engineering, Halmstad University, Box 823, SE-301 18 Halmstad, Sweden

Keywords: Nanowire, radial, quantum well, STEM-EDX, light-emitting diodes, MOCVD

Nanowires have the potential to play an important role for next-generation light-emitting diodes. In this work we present a growth scheme for radial nanowire quantum-well structures in the AlGaInP material system using a GaInP nanowire core as a template for radial growth with GaInP as the active layer for emission and AlGaInP as charge carrier barriers. The different layers were analyzed by x-ray diffraction to ensure

21 lattice-matched radial structures. Furthermore we evaluated the material composition
22 and hetero-junction interface sharpness by scanning transmission electron microscopy
23 energy dispersive x-ray spectroscopy. The electro-optical properties were investigated
24 by injection luminescence measurements. The presented results can be a valuable track
25 towards radial nanowire light-emitting diodes in the AlGaInP material system in the
26 red/orange/yellow color spectrum.

27

28 Nanowires (NWs) are future building blocks for optoelectronic devices such as
29 solar cells,[1] transistors[2] and light-emitting diodes.[3] Due to the small dimensions, NWs
30 can exhibit different electronic and optical properties as compared to planar structures
31 of the same materials. Material combinations that are incompatible in planar structures
32 can be used in NWs, allowing more freedom in bandgap tuning of active segments to
33 desired wavelengths in NW based devices.

34 It is a common practice in III-As/P planar light-emitting diode structures to use
35 GaInP as the active layer.[4-18] By introducing Al in GaInP, the bandgap can be increased
36 all the way to 2.52 eV in AlP, but which has an indirect bandgap.[19] The Al/Ga ratio in
37 lattice-matched AlGaInP can be tuned to be used as electron blocking layer keeping the
38 (AlGa)/In ratio constant since the lattice constant changes only slightly with increasing
39 Al due to similar lattice constants for AlP and GaP.[19, 20] In planar structures, LEDs
40 based on the AlGaInP material system are often grown on GaAs substrates, since
41 $(Al_xGa_{1-x})_{0.51}In_{0.49}P$ is lattice-matched to GaAs.[19] After synthesis, the GaAs substrate is
42 replaced by a transparent GaP substrate via ”wafer-bonding”.[21-24] Alternatively, in order
43 to grow $Ga_{0.47}In_{0.53}P$ which leads to red light emission[25] on GaP, graded buffer layers
44 are needed to adjust for the 3.6 % lattice mismatch.[19, 20] Graded buffer layers usually

45 exhibit dislocations which lead to efficiency losses. Therefore the possibility to achieve
46 desired bandgaps is limited. In the NW geometry, the desired composition can be grown
47 directly on substrates with different lattice constants because of the small NW
48 footprint[26, 27] and due to effective strain relaxation via the free surfaces in NWs. For
49 designing radial NW structures lattice matching requirements become more relevant,
50 and the NW core can be used as a "substrate" for growing NW shells that are lattice-
51 matched with the NW core. Radial core-shell NWs have been shown to be a versatile
52 structure for light-emitting diodes[28, 29] because of the larger junction area as compared
53 to axial NW structures. Several contributions on radial NW quantum-well (QW)
54 structures with emission in the infrared (IR) color spectrum based on various material
55 systems have been reported such as GaP/GaAs/GaInP,[30] InP/InAsP/InP,[31, 32]
56 InP/InAs/InP[33, 34] and GaAs/AlGaAs.[35-38] Moreover, radial NW QWs in the short-
57 wavelength visible spectrum with GaN/InGaN/GaN[28, 29, 39] as well as multi-quantum-
58 well (MQW) structures in (In)AlN/GaN[40, 41] emitting in the ultra-violet (UV) region
59 have been reported. Here, we report the growth and characterization of radial NW p-i-n
60 junctions in the AlGaInP material system designed for the long-wavelength visible
61 spectrum. We grow untapered GaInP NW cores on a GaP substrate and use the NW
62 core as a template for radial growth of materials with composition optimized for red
63 light emission. After growing a radial QW structure, the material composition is
64 analyzed, and the effect of different n-type dopant precursors on the growth dynamics is
65 studied. We observe Al enrichment in the corners of the AlGaInP layers in the cross-
66 section perpendicular to the NW axis by use of transmision electron microscopy (TEM).
67 Electrical measurements confirm the presence of a pn-junction and electrical injection
68 results in luminescence in the red color spectrum.

69 P-doped ($\bar{1}\bar{1}\bar{1}$)B GaP wafers were deposited with a 20 nm thick silicon nitride
70 (SiN_x) layer via plasma-enhanced chemical vapor deposition (PECVD). Resist-spinning
71 with a bi-layer method,[42] nanoimprint lithography (IPS/STU process[43]), reactive ion
72 etching (RIE), Au evaporation and lift-off were used to define the template for NW
73 growth. The template consists of a hexagonal pattern of circular holes of 100 nm with a
74 pitch of 1 µm. The deposited Au layer thickness was 10 nm. The material design of the
75 p-type GaInP NW core was reported elsewhere.[44] In short, the core consists of a GaP
76 stub, a GaInP transition segment where the Ga content decreases from p-GaP to p-
77 GaInP of the composition intended for the NW and a long p-GaInP segment with
78 homogenous material composition. The complete radial structure is formed by
79 depositing several additional shell layers on the core: a p-GaInP buffer layer (15 s
80 growth time), a p-AlGaInP cladding layer (30 s), an intrinsic GaInP layer (15 s) as the
81 active layer for carrier recombination, an n-AlGaInP cladding layer (30 s) and an n-
82 GaInP layer (2 min) which is intended to be highly doped for electrical contacts (Figure
83 1). The p-GaP wafer below the shells is passivated by the SiN_x mask in order to make
84 more precursor material contribute to NW growth and avoid substrate leakage currents
85 from the outermost shell directly into the substrate in device configuration. The NWs
86 were grown by metal-organic chemical vapor deposition (MOCVD) in an Aixtron 200/4
87 reactor at a pressure of 100 mbar for the core and 50 mbar for the shells. The precursors
88 were trimethylaluminum (TMAl), trimethylgallium (TMG), trimethylindium (TMI),
89 phosphine (PH_3) as well as diethyl zinc (DEZn) for p-type doping and triethyltin (TESn)
90 or hydrogen sulfide (H_2S) for n-type doping, respectively, in a total flow of 13 l/min
91 using hydrogen (H_2) as carrier gas. Hydrogen chloride (HCl) was used to impede radial
92 growth during the synthesis of the NW core.[45-48] The molar fractions for growth of the

93 p-GaInP segment of the core at 440 °C were $\chi_{TMG} = 6.724\times10^{-5}$, $\chi_{TMI} = 1.228\times10^{-5}$, χ_{PH3}
94 $= 4.6\times10^{-3}$, $\chi_{DEZn} = 3.13\times10^{-6}$ and $\chi_{HCl} = 6.154\times10^{-5}$. After growth of the NW core with
95 a length of 1.5 µm and cooling the reactor under a PH_3/H_2 mixture, the sample was
96 taken out of the reactor and the gold alloy particle removed by a two-step wet chemical
97 etch process in order to impede catalyzed axial growth during shell growth using
98 H_2SO_4:H_2O (1:10) and KI:I_2:H_2O (4 g : 1 g : 40 ml),[49-51] both for 10 s. After loading the
99 sample back into the reactor, it was heated to 650 °C and the sample was annealed for 4
100 min under a PH_3/H_2 mixture to remove any oxides on the NW core surface. The shell
101 growth of the different layers, at 650 °C, was initialized/terminated by switching on/off
102 the respective group III and dopant precursor sources. The molar fractions of TMI, PH_3
103 and DEZn during shell growth were $\chi_{TMI} = 3.509\times10^{-5}$, $\chi_{PH3} = 1.54\times10^{-2}$ and $\chi_{DEZn} =$
104 3.13×10^{-6}, respectively. For every shell we performed a series of growth experiments on
105 different samples from the same NW core growth run with varying χ_{TMG} for the GaInP
106 shells and a varying sum ($\chi_{TMAl} + \chi_{TMG}$) for the AlGaInP shells (but keeping the χ_{TMAl} /
107 ($\chi_{TMAl} + \chi_{TMG}$) ratio constant), respectively, in order to achieve lattice-matched
108 compositions between all layers. The molar fractions for TMAl, TMG and the n-type
109 dopants for lattice-matched layers are shown in Table S1. Applying growth parameters
110 for lattice-matched layers using H_2S as n-type dopant, we performed five growth runs
111 with different χ_{TMAl} / ($\chi_{TMAl} + \chi_{TMG}$) ratios (but with constant sum ($\chi_{TMAl} + \chi_{TMG}$))
112 (Table S2) to evaluate the correlation between the group III precursor molar fractions in
113 the gas phase and the Al concentration in the AlGaInP crystal (Table S2). After shell
114 growth, the sample was cooled down to room temperature under a PH_3/H_2 mixture.
115
116

117
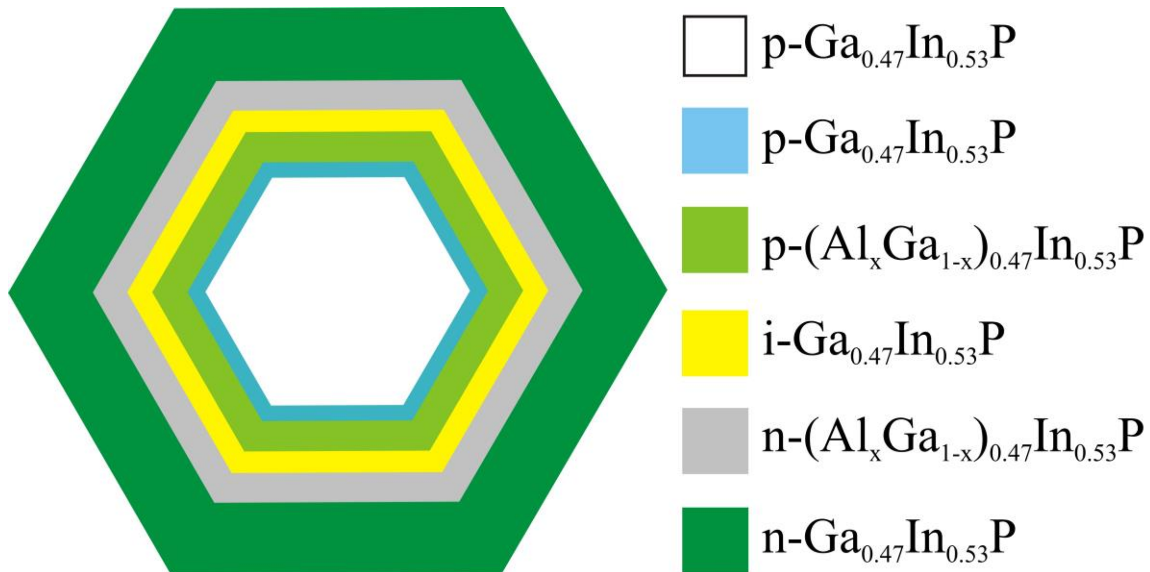

118 **Figure 1.** Schematic construction of the grown radial GaInP/AlGaInP/GaInP NWs. The
119 different colors indicate the strain-free layers with desired compositions during the
120 development of the radial structure. The white area in the center is the NW core.

121

122 Scanning electron microscopy (SEM) was used to characterize the length,
123 diameter and surface morphology of over 30 NWs in the center of each sample.

124 In order to determine the ratio between Ga and In in GaInP shells and between
125 (Al+Ga) and In in AlGaInP shells, respectively, x-ray diffraction (XRD)
126 characterization was used. The measurements reveal the composition range in a large
127 amount of NWs from the probed area of the sample corresponding to a few mm^2. Each
128 shell in Figure 1 was characterized individually. After optimization of the p-GaInP
129 shell, the neighboring p-AlGaInP shell was developed according to XRD measurements
130 and so on. Most of these measurements were done during developing a procedure to
131 grow ternary GaInP NW with homogeneous material composition by ramping χ_{TMI} up
132 by 25 % during a growth time of 4 min.[44] Therefore most of the NW cores, except the
133 ones with S-doped n-GaInP shells, had an inhomogeneous composition along the axial

134 direction of the NW. In order to determine the material composition, the shell under
135 investigation was grown 4-6 times longer than in the final structure in order to get a
136 proper XRD signal from the respective shell which by volume is dominated by the shell
137 under evaluation although it contains the signal from the entire NW (including the broad
138 XRD signal from the NW core). According to Schubert[25] GaInP has a bandgap between
139 1.65 and 1.99 eV in the red color spectrum, which corresponds to an XRD angle
140 between 27 and 27.4 degrees for 2 Theta for a crystal growing in $(\bar{1}\bar{1}\bar{1})$B direction. For
141 each shell the composition was aimed at $Ga_{0.47}In_{0.53}P$ and $(Al_xGa_{1-x})_{0.47}In_{0.53}P$,
142 respectively, which for GaInP corresponds to a bandgap of 1.82 eV[25] and for the NW
143 core and all shells to an XRD angle 2 Theta of 27.2 degrees.

144 The NWs were studied by TEM analysis in a probe corrected FEI Titan 80-300
145 ATEM. Cross-sectional TEM specimens from five samples grown with different χ_{TMAl} /
146 (χ_{TMAl} + χ_{TMG}) ratios in the AlGaInP layers were prepared using focused ion beam
147 (FIB) milling. All the TEM specimens were prepared perpendicular to the axial NW
148 axis of the full core-shell structure (including all layers) in the middle of the axial
149 elongation of the NWs. To study the structure and map the compositional distribution in
150 the NWs, atomic resolution scanning TEM (STEM) and high-angle annular dark-field
151 STEM (HAADF STEM) together with energy dispersive x-ray spectroscopy (EDX)
152 were performed.

153 In order to optimize the structure for injection luminescence (IL) measurements,
154 we further developed the epitaxial structure. The growth time for the upper segment of
155 the p-GaInP NW core was increased to 6 min to get 1.8-2 µm long NWs and
156 consequently the ramping range for χ_{TMI} increased to about 50 %,[44] which resulted in a
157 ternary p-type $Ga_{0.47}In_{0.53}P$ NW core with homogeneous material composition. On top

158 of the p-GaInP NW core an n-GaP top segment was added in order to avoid leakage
159 from the outermost shell directly into the NW core. The p-GaInP buffer layer
160 (innermost shell) was grown thicker (2 min growth time instead of 15 s) to fill any
161 possible gap between the NW core and SiN_x mask opening and therefore to avoid any
162 current leakage from the QW directly into the substrate. The AlGaInP barriers were
163 grown non-intentionally doped instead of previously p- and n-doped during the
164 development of lattice-matched NW shells. The highest χ_{TMAl} / (χ_{TMAl} + χ_{TMG}) ratio of
165 0.63 out of five different growth runs (Table S2) was used to have the highest possible
166 AlGaInP barrier height of our series. Thus the carriers are even more effectively trapped
167 in the QW. For the i-GaInP QW, we made a series of three different growth times (15,
168 30 and 60 s). Preliminary IV-measurements indicated higher rectification ratios using
169 tin (Sn) in the outermost shell as compared to sulphur (S), similar to InP core-shell NW
170 pn-junctions.[50, 52] Therefore we doped the outermost n-GaInP shell with Sn and
171 increased χ_{TESn} to 1.314×10^{-5}.

172 In order to assess the electrical properties of the NWs, 100×100 μm^2 large test
173 LED devices were fabricated. UV lithography and wet etching were used to define the
174 device area and the transparent electrical contacts to the NW shells were fabricated by
175 sputtering indium-tin-oxide (ITO) on the NWs, whereas the NW cores were electrically
176 contacted via the p-type substrate.[52]

177 A probe station was used for measuring IV curves (Figure 4b) at room
178 temperature, whereas IL measurements (Figure 4d) were carried out in another setup - at
179 room temperature as well - in which the outcoming light was collected and measured by
180 a fiber spectrometer. Special care was taken that the relative position between the

181 detector and the sample was identical for different samples in order to compare the light
182 intensity.

183 In order to develop a process flow for growing NWs with a radial geometry, it is
184 crucial to design and optimize the growth parameters for each layer in the structure
185 separately. Thereby we analyze the material composition for each layer as a function of
186 group III precursor molar fractions and aim at strain-free NW shells with compositions
187 of $Ga_{0.47}In_{0.53}P$ and $(Al_xGa_{1-x})_{0.47}In_{0.53}P$ for GaInP and AlGaInP layers shown in Figure
188 1. The p-GaInP buffer layer is used for re-nucleation, in order to overcome any potential
189 surface defects with respect to morphology during wet-etching of the gold alloy particle.
190 XRD measurements show that a crystal composition of $Ga_{0.47}In_{0.53}P$ (XRD angle 2
191 Theta = 27.2°) can be achieved by tuning χ_{TMG} to 3.812×10^{-5} (Figure 2a). Figure 2b
192 shows the composition of the p-GaInP layer as a function of χ_{TMG} calculated based on
193 XRD measurements.

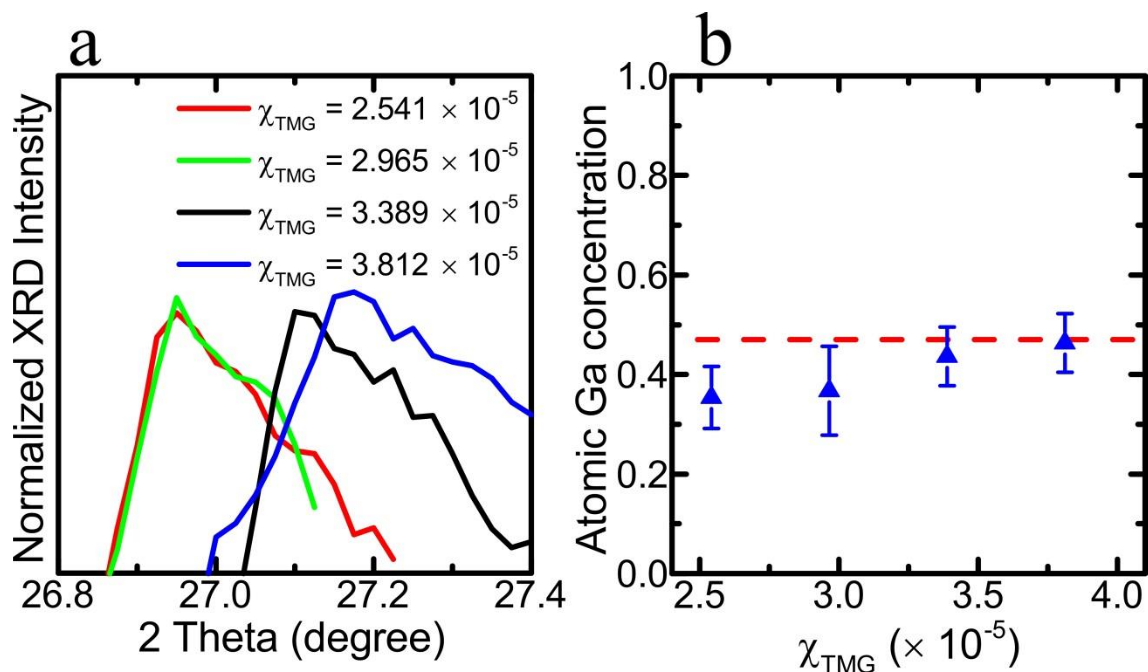

194

195 **Figure 2.** (a) XRD graph for the p-GaInP NW shell layer depending on different χ_{TMG}.
196 2 Theta was aimed at 27.2° which corresponds to a composition of $Ga_{0.47}In_{0.53}P$. The

197 signal for the two lower molar fractions is cut outside the peak for visibility reasons.
198 The GaP substrate peak is at 28.34°. (b) Atomic Ga concentration for the p-GaInP layer
199 as a function of χ_{TMG}. The error bars indicate the composition range which was
200 determined with the FWHM.[44] The dashed line shows the desired composition
201 $Ga_{0.47}In_{0.53}P$ which corresponds to an XRD 2 Theta degree of 27.2°.

202

203 As stated earlier, most NW cores had an inhomogeneous material composition[44]
204 during the development of lattice-matched shells. Especially for the p-GaInP and p-
205 AlGaInP shell, the composition of the "upper segment" of the core varied from
206 $Ga_{0.3}In_{0.7}P$ to $Ga_{0.44}In_{0.56}P$, which was determined with the full-width-at-half-maximum
207 (FWHM)[44] of the XRD signal for the NW core. Also for the NW shells we observe a
208 broader XRD signal than what is typically observed for completely homogeneous
209 ternary NW materials,[44] which indicates that the NW shell growth also results in an
210 inhomogeneous composition along the axial direction of the NW shell. The growing
211 layer tends to adopt the lattice spacing of the underlying layer and the XRD signal
212 contains all compositions along the axial direction of the NW shells.

213 For the barriers p- and n-AlGaInP we note that AlGaInP can be treated as a
214 combination of AlInP and GaInP. We found out by XRD measurements during
215 optimizing the composition of the p- and n-AlGaInP layers that by adding χ_{TMAl} while
216 keeping the χ_{TMG} and χ_{TMI} at the same value as for the p-GaInP shell, the composition
217 shifts towards a more Al/Ga rich AlGaInP layer as compared to In. Therefore we had to
218 use a lower χ_{TMG} with respect to the previous p-GaInP layer to achieve lattice-matching.
219 If we assume that the Ga and In atoms from the respective precursor molecules are
220 similarly incorporated into AlGaInP as for the p-GaInP layer, then the addition of Al

221 would by volume result in a higher growth rate. However, we cannot rule out that TMAl
222 reduces the diffusion length of In species, not only dilutes them, and that some Ga
223 atoms are replaced by Al atoms.

224 The intrinsic GaInP QW layer was grown with the same precursor molar
225 fractions as for the p-GaInP layer since Zn did not affect the composition for shell
226 growth, in agreement with thin-film growth.[53, 54]

227 For the two n-type layers, two different dopants - Sn and S - were investigated
228 independently of each other. The n-type dopant precursor molar fraction was 6 (5.4)
229 times higher for χ_{TESn} (χ_{H2S}) in the n-GaInP layer than in the n-AlGaInP layer since the
230 outermost layer is intended to be electrically contacted. In case of Sn, χ_{TMAl} and χ_{TMG}
231 had to be reduced by 20 % for the n-AlGaInP layer compared to the p-AlGaInP layer
232 and χ_{TMG} by 11 % for the n-GaInP layer compared to the p- and i-GaInP layers,
233 respectively, in order to achieve lattice-matching. For n-type doping with S, we did not
234 observe any large shift in composition upon doping.

235 Figure S1 shows the morphology of the n-GaInP outermost shells, doped with
236 Sn (Figure S1a) and S (Figure S1b), respectively, and intrinsic shells for comparison
237 (Figure S1c). The use of TESn leads to the formation of Sn-rich particles on the side
238 facets, similar to n-type shell doping by Sn of GaP[51] and InP[50] core-shell NW pn-
239 junctions. Also for S doping we see several irregularities on the morphology of the
240 surface but the effect is much weaker than for Sn. The NWs with the intrinsic two
241 outermost shells are up to 15 % thicker than the n-type shells doped with Sn or S (not
242 visible in low magnification SEM images in Figure S1), probably because Sn forms a
243 surface accumulation layer[55] and S acts as a surface passivator.[56-58] Table S1 shows the

244 molar fractions of the precursors during shell growth except for TMI, PH_3 and DEZn
245 (for p-doping) since they were kept constant.

246 The compositional distribution across the entire NW cross-section,
247 perpendicular to the axial axis of the NWs, was investigated using STEM-EDX. The
248 different radially grown layers are visible in the HAADF STEM image in Figure 3a,
249 where the second highest χ_{TMAl} / (χ_{TMAl} + χ_{TMG}) ratio out of five different runs (Table
250 S2) was used. The atomic resolution HAADF image (inset of Figure 3a) shows
251 relatively sharp hetero-interfaces with inter-diffusion of a few atomic layers, indicating
252 no or only small group III intermixing occurs at the hetero-interfaces. The calculated
253 material compositions from the STEM-EDX measurements for each segments across
254 the NW are shown in Figure 3d.

255 The segments in [110] direction (normal of the “m-plane”) are relatively
256 homogeneous in composition with a slight In overweight in the i-GaInP QW layer, close
257 to the intended material compositions $Ga_{0.47}In_{0.53}P$ and $(Al_xGa_{1-x})_{0.47}In_{0.53}P$. However, in
258 [112] direction (in the corners of the hexagon), there are segments with higher Al
259 content in the p- and n-AlGaInP layers which can be seen as black stripes in Figure 3a.

260 STEM-EDX elemental mapping of the NW composition confirmed Al rich
261 corners in AlGaInP and even Ga rich corners in i- and n-GaInP (Figure 3b). It showed
262 relative radial uniformity only for the p-GaInP buffer layer. Starting from the p-
263 AlGaInP layer towards the outer shells, we observe areas in the six corners in [112]
264 direction with higher Al or Ga contents than in [110] direction. Al aggregates in the
265 corners of the quaternary shells and this phenomenon propagates through to the
266 respective outside lying neighboring shell all the way to the outermost n-GaInP shell.
267 The Ga rich corners in the i- and n-GaInP shells are likely to be formed due to

268 thermodynamic arguments. The atomic radius of Ga (130 pm) is far closer to the atomic
269 radius of Al (125 pm) than In (155 pm), therefore, for Ga atoms it might be more
270 favorable to deposit next to Al rich corners than next to the AlGaInP facets in [110]
271 direction. In other words, a layer tends to adopt the lattice constant of the neighboring
272 layer upon epitaxial processes. During XRD measurements for the separate layers, we
273 found a relatively broad signal for all shells except for the p-GaInP shell. This could be
274 caused - besides the NW core material composition inhomogeneity in axial direction -
275 by the two different types of segments with different lattice constants in [110] and [112]
276 direction. Al rich vertices of a hexagon have also been observed in other core-shell NW
277 structures such as GaAs/AlInP[59, 60] as well as GaAs/AlGaAs[35-38, 61, 62] and
278 InAlN/GaN/InAlN[40] MQWs.

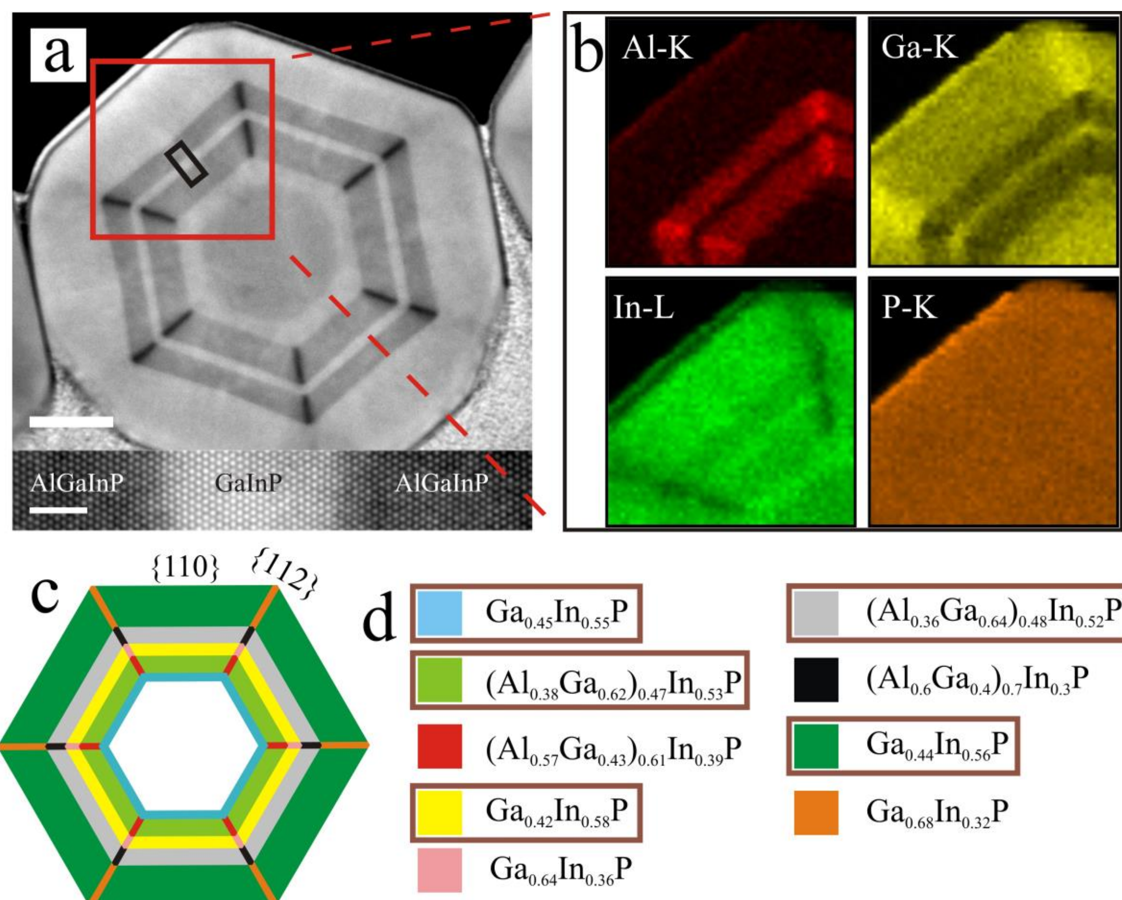

279

280 **Figure 3.** Cross-section images perpendicular to the axial NW axis of radial
281 GaInP/AlGaInP/GaInP core-shell NWs with two AlGaInP layers as barriers where the
282 ratio χ_{TMAl} / (χ_{TMAl} + χ_{TMG}) was 0.55. (a) HAADF STEM image of a FIB-prepared
283 cross-sectional specimen of the whole core-shell NW (the scale bar is 50 nm). The
284 cross-section was taken in the middle of the axial elongation of the NW. The inset
285 shows an atomic resolution STEM image of the GaInP/AlGaInP/GaInP interface from
286 the area in image a marked with a black rectangle (the scale bar in the inset is 2 nm). (b)
287 STEM-EDX maps from the area marked with the red square in the HAADF image,
288 showing the Al, Ga, In and P distribution. (c) schematic cross-section image. The colors
289 indicate different compositions which are calculated in image d. (d) Material
290 composition of different regions of the NW, calculated from the EDX measurements.
291 All segments in [110] direction are nearly lattice-matched and marked with a brown
292 frame.

293

294 Sköld *et al.*[59] analyzed Al rich corners in AlInP shells and argued that Al
295 aggregates at the {112} facets because In adatoms have a longer diffusion length than
296 Al adatoms. In adatoms can therefore diffuse away from areas with high surface
297 energies more easily and we believe the same is true here for our quaternary AlGaInP
298 NW shells. Wagner *et al.*[60] derived this phenomenon more in detail using surface
299 curvature where the adatoms diffuse toward the lower chemical potential. Phase
300 segregation has recently also been demonstrated in III-V-V ternary GaAsP core-shell
301 NWs with P enrichment in the corners of the hexagon.[63] The authors argue that the
302 small {112} facets have a curvature-induced high surface chemical potential, which

303 makes it easier for the group V element arsenic (As) to diffuse away from the {112}
304 facets because of the longer diffusion length of its adatoms.[63]

305 The fact that the corners of the hexagon are Al/Ga richer as compared to In
306 means that the bandgap of the segments in [112] direction is higher. Thus, carriers will
307 preferably tend to diffuse to the lower-bandgap [110] direction, which means that the
308 lower-bandgap areas become recombination centers. The segments with smaller lattice
309 constants and higher bandgaps do not attract electrons, which would decrease the
310 recombination efficiency by strain-induced non-radiative recombination.

311 In order to demonstrate the potential of the GaInP/AlGaInP/GaInP core-shell
312 NWs for a radial NW LED, we evaluated their electro-optical properties. The χ_{TMAl} /
313 ($\chi_{TMAl} + \chi_{TMG}$) precursor ratio of 0.63 for the AlGaInP barriers (Figure S2) resulted in a
314 barrier height (conduction band offset) of about 118-194 meV (calculated after atomic
315 concentrations from STEM-EDX measurements and refs.[64-66] where $(Al_xGa_{1-x})_yIn_{1-y}P$
316 lattice-matched to GaAs was used (y=0.51 according to ref.[19])). The series of three
317 different growth times for the i-GaInP QW resulted in thicknesses of 5, 10 and 20 nm
318 (estimated by the STEM image in Figure 3a where the QW thickness was about 5 nm
319 for a growth time of 15 s).

320 For the 20 nm thick QWs the IL signal from 100×100 μm^2 large devices is
321 relatively weak with a peak at 1.75-1.8 eV (Figure 4a), which corresponds well to a
322 band-to-band electron-hole pair recombination with the bandgap of $Ga_{0.42}In_{0.58}P$ at 1.79
323 eV[19] where a bowing factor of 0.65 eV for the Γ-band at 300 K was used[19] or 1.75 eV.[25]
324 For thinner QWs we observe a slight blue-shift of the IL peak which we attribute to
325 quantization. For 5 nm QW thickness the peak is broader than for 10 nm, which can be
326 attributed to transitions from the quantized state and the ground state of the conduction

band to the valence band. We find the highest IL intensity for a QW thickness of 10 nm (Figure 4a).

The IV curve in Figure 4b represents the electrical performance of the NW LED device with a 10 nm thick QW. This device has a threshold voltage of approximately 3 V, above which the NW LED starts to emit red light visible to the eye (Figure 4d). The peak intensity increases with the current level (Figure 4c) and does not show any shift in energy. In reverse bias the device shows a current of 17 mA at -3 V until breakdown occurs at about -4 V.

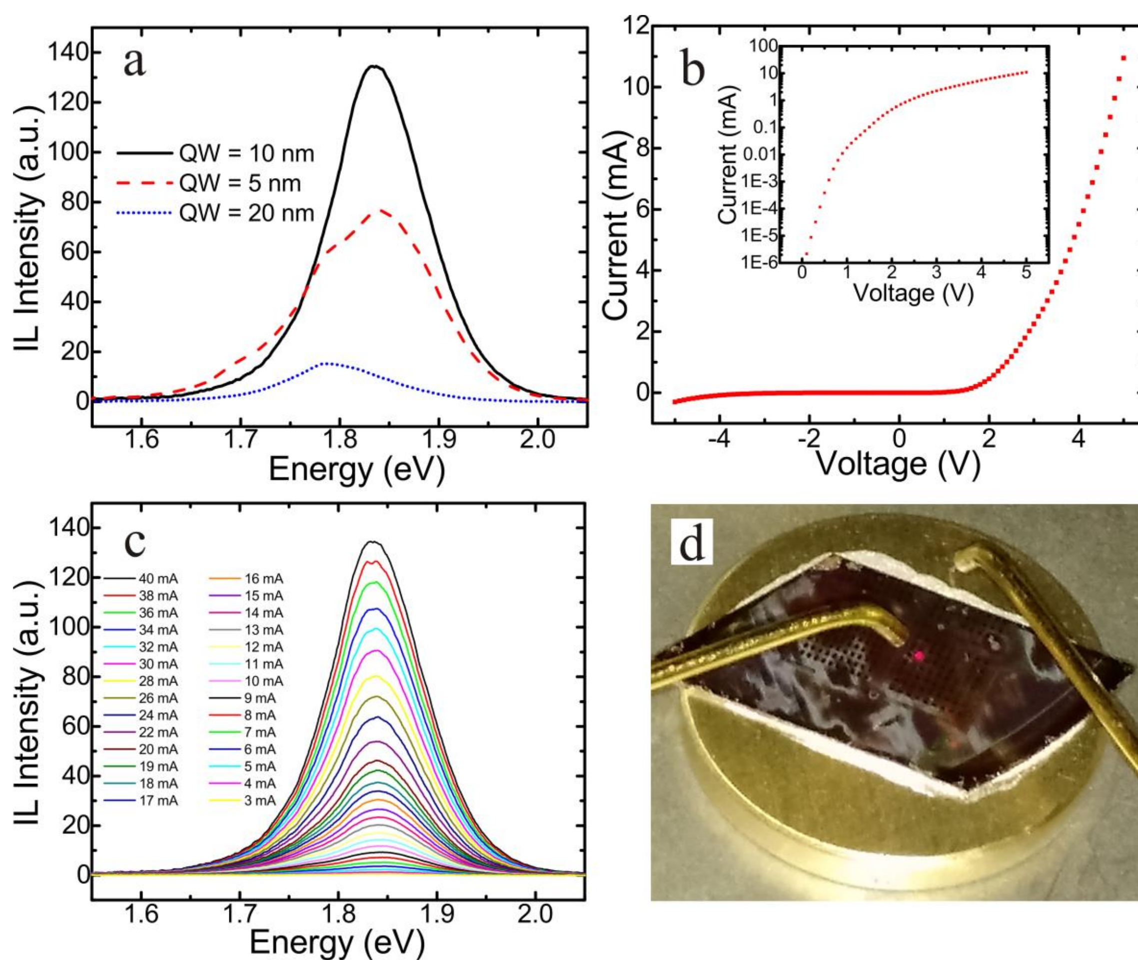

Figure 4. IL measurements on different radial GaInP/AlGaInP/GaInP core-shell NW LED devices. In all 4 images, graphs from the same device with 10 nm QW thickness are shown (image a shows IL spectra of two additional devices). (a) IL spectra of 3

339 devices with different QW thicknesses at 40 mA as a function of the emission energy.
340 (b) IV characteristics. (c) IL spectra for a series of different currents as a function of the
341 energy. (d) photo of the red light emission of the sample in the probe station at a
342 forward bias of about 3 V.

343 In conclusion, we have presented an epitaxial growth scheme about a radial p-i-n
344 junction nanowire quantum well structure in the AlGaInP material system with GaInP
345 as the active layer. The n-type dopant Sn slightly changes the composition towards In
346 richer material. The material composition of each layer was determined by STEM-EDX.
347 We find Al rich corners in AlGaInP and relate that to a short diffusion length of Al
348 adatoms. Finally we demonstrated the electro-optical properties of the NW light-
349 emitting diode devices. They illuminate with red color at a forward bias of around 3 V.

350 ASSOCIATED CONTENT

351 **Supporting Information**

352 Additional growth parameters. Morphology of the NW side facets for different n-type
353 dopants. Al content *x* of the p-AlGaInP:Zn and n-AlGaInP:S barriers in $(Al_xGa_{1-x})InP$.
354 PL spectrum of a single NW with 10 nm QW thickness. This material is available free
355 of charge via the Internet at http://pubs.acs.org.

356

357 AUTHOR INFORMATION

358 **Corresponding Author**

359 * magnus.borgstrom@ftf.lth.se

360

361 **Present Address**

362 ⊥Department of Materials Science and NanoEngineering, Rice University, 6100 Main
363 Street MS-325, Houston, TX 77005, United States

364

365 **Author Contributions**

366 The manuscript was written through contributions of all authors. All authors have given
367 approval to the final version of the manuscript.

368

369 **Notes**

370 The authors declare no competing financial interest.

371

372 ACKNOWLEDGMENT

373 This work was performed within NanoLund and supported by the Swedish Research
374 Council (Vetenskapsrådet), the Swedish Foundation for Strategic Research (SSF), by
375 the Knut and Alice Wallenberg Foundation, and by the EU program NWs4Light under
376 grant 280773.

377 REFERENCES

378

379 1. Wallentin, J.; Anttu, N.; Asoli, D.; Huffman, M.; Åberg, I.; Magnusson, M. H.;
380 Siefer, G.; Fuss-Kailuweit, P.; Dimroth, F.; Witzigmann, B.; Xu, H. Q.; Samuelson, L.;
381 Deppert, K.; Borgström, M. T. *Science* **2013,** 339, (6123), 1057-1060.
382 2. Tomioka, K.; Yoshimura, M.; Fukui, T. *Nature* **2012,** 488, (7410), 189-192.
383 3. Gudiksen, M. S.; Lauhon, L. J.; Wang, J.; Smith, D. C.; Lieber, C. M. *Nature*
384 **2002,** 415, (6872), 617-620.
385 4. Wirth, R.; Karnutsch, C.; Kugler, S.; Streubel, K. *Ieee Photonic Tech L* **2001,**
386 13, (5), 421-423.
387 5. Sigai, A. G.; Nuese, C. J.; Enstrom, R. E.; Zamerowsi, T. *J Electrochem Soc*
388 **1973,** 120, (7), 947-955.
389 6. Nuese, C. J.; Sigai, A. G.; Abrahams, M. S.; Gannon, J. J. *J Electrochem Soc*
390 **1973,** 120, (7), 956-965.
391 7. Nuese, C. J.; Sigai, A. G.; Gannon, J. J.; Zamerowsi, T. *J Electron Mater* **1974,**
392 3, (1), 51-78.
393 8. Stinson, L. J.; Yu, J. G.; Lester, S. D.; Peanasky, M. J.; Park, K. *Applied Physics*
394 *Letters* **1991,** 58, (18), 2012-2014.
395 9. Kondo, S.; Matsumoto, S.; Nagai, H. *Applied Physics Letters* **1988,** 53, (4), 279-
396 281.
397 10. Ermakov, O. N.; Garba, L. S.; Golovanov, Y. A.; Sushkov, V. P.; Chukichev, M.
398 V. *Ieee T Electron Dev* **1979,** 26, (8), 1190-1193.
399 11. Chang, S. J.; Chang, C. S. *Japanese Journal of Applied Physics Part 2* **1998,** 37,
400 (6A), L653-L655.
401 12. Chang, S. J.; Chang, C. S. *Ieee Photonic Tech L* **1998,** 10, (6), 772-774.
402 13. Greger, E.; Gulden, K. H.; Riel, P.; Schweizer, H. P.; Moser, M.; Schmiedel, G.;
403 Kiesel, P.; Dohler, G. H. *Applied Physics Letters* **1996,** 68, (17), 2383-2385.
404 14. Marmalyuk, A. A.; Gorlachuk, P. V.; Ryaboshtan, Y. L.; Brudnyi, V. N.;
405 Prudaev, I. A.; Romanov, I. S.; Lelekov, M. A. *Russ Phys J+* **2013,** 56, (8), 894-897.
406 15. McGill, L.; Wu, J. W.; Fitzgerald, E. A. *Journal of Applied Physics* **2004,** 95,
407 (12), 7561-7566.
408 16. Dawson, M. D.; Duggan, G. *Applied Physics Letters* **1994,** 64, (7), 892-894.
409 17. Lee, C. Y.; Wu, M. C.; Lin, W. *Journal of Crystal Growth* **1999,** 200, (3-4),
410 382-390.
411 18. Rooman, C.; Windisch, R.; D'Hondt, M.; Dutta, B.; Modak, P.; Mijlemans, P.;
412 Borghs, G.; Vounckx, R.; Moerman, I.; Kuijk, M.; Heremans, P. *Electron Lett* **2001,** 37,
413 (13), 852-853.
414 19. Vurgaftman, I.; Meyer, J. R.; Ram-Mohan, L. R. *Journal of Applied Physics*
415 **2001,** 89, (11), 5815-5875.
416 20. Physical Properties of Semiconductors, Ioffe Institute, Sankt Petersburg, Russia;
417 http://www.ioffe.ru/SVA/NSM/Semicond/.
418 21. Kish, F. A.; Steranka, F. M.; Defevere, D. C.; Vanderwater, D. A.; Park, K. G.;
419 Kuo, C. P.; Osentowski, T. D.; Peanasky, M. J.; Yu, J. G.; Fletcher, R. M.; Steigerwald,
420 D. A.; Craford, M. G.; Robbins, V. M. *Applied Physics Letters* **1994,** 64, (21), 2839-
421 2841.
422 22. Höfler, G. E.; Vanderwater, D. A.; DeFevere, D. C.; Kish, F. A.; Camras, M. D.;
423 Steranka, F. M.; Tan, I. H. *Applied Physics Letters* **1996,** 69, (6), 803-805.

424 23. Gardner, N. F.; Chui, H. C.; Chen, E. I.; Krames, M. R.; Huang, J. W.; Kish, F.
425 A.; Stockman, S. A.; Kocot, C. P.; Tan, T. S.; Moll, N. *Applied Physics Letters* **1999,**
426 74, (15), 2230-2232.
427 24. Dakin, J.; Brown, R. G. W., *Handbook of Optoelectronics - Volume I*. Taylor &
428 Francis: New York, 2006.
429 25. Schubert, E. F., *Light-emitting diodes*. 2nd ed.; Cambridge University Press:
430 Cambridge; New York, 2006.
431 26. Mårtensson, T.; Svensson, C. P. T.; Wacaser, B. A.; Larsson, M. W.; Seifert,
432 W.; Deppert, K.; Gustafsson, A.; Wallenberg, L. R.; Samuelson, L. *Nano Letters* **2004,**
433 4, (10), 1987-1990.
434 27. Roest, A. L.; Verheijen, M. A.; Wunnicke, O.; Serafin, S.; Wondergem, H.;
435 Bakkers, E. P. A. M. *Nanotechnology* **2006,** 17, (11), S271-S275.
436 28. Qian, F.; Li, Y.; Gradečak, S.; Wang, D. L.; Barrelet, C. J.; Lieber, C. M. *Nano*
437 *Letters* **2004,** 4, (10), 1975-1979.
438 29. Qian, F.; Gradečak, S.; Li, Y.; Wen, C. Y.; Lieber, C. M. *Nano Letters* **2005,** 5,
439 (11), 2287-2291.
440 30. Svensson, C. P. T.; Mårtensson, T.; Tragårdh, J.; Larsson, C.; Rask, M.;
441 Hessman, D.; Samuelson, L.; Ohlsson, J. *Nanotechnology* **2008,** 19, (30), 305201.
442 31. Kawaguchi, K.; Sudo, H.; Matsuda, M.; Takemoto, K.; Yamamoto, T.;
443 Arakawa, Y. *Applied Physics Letters* **2015,** 106, (1), 012107.
444 32. Kawaguchi, K.; Sudo, H.; Matsuda, M.; Ekawa, M.; Yamamoto, T.; Arakawa,
445 Y. *Japanese Journal of Applied Physics* **2015,** 54, (4S), 04DN02.
446 33. Hiruma, K.; Tomioka, K.; Mohan, P.; Yang, L.; Noborisaka, J.; Hua, B.;
447 Hayashida, A.; Fujisawa, S.; Hara, S.; Motohisa, J.; Fukui, T. *Journal of*
448 *Nanotechnology* **2012,** 2012, 29.
449 34. Mohan, P.; Motohisa, J.; Fukui, T. *Applied Physics Letters* **2006,** 88, (13),
450 133105.
451 35. Mancini, L.; Fontana, Y.; Conesa-Boj, S.; Blum, I.; Vurpillot, F.; Francaviglia,
452 L.; Russo-Averchi, E.; Heiss, M.; Arbiol, J.; Fontcuberta i Morral, A.; Rigutti, L.
453 *Applied Physics Letters* **2014,** 105, (24), 243106.
454 36. Heiss, M.; Fontana, Y.; Gustafsson, A.; Wust, G.; Magen, C.; O'Regan, D. D.;
455 Luo, J. W.; Ketterer, B.; Conesa-Boj, S.; Kuhlmann, A. V.; Houel, J.; Russo-Averchi,
456 E.; Morante, J. R.; Cantoni, M.; Marzari, N.; Arbiol, J.; Zunger, A.; Warburton, R. J.;
457 Morral, A. F. I. *Nat Mater* **2013,** 12, (5), 439-444.
458 37. Fickenscher, M.; Shi, T.; Jackson, H. E.; Smith, L. M.; Yarrison-Rice, J. M.;
459 Zheng, C. L.; Miller, P.; Etheridge, J.; Wong, B. M.; Gao, Q.; Deshpande, S.; Tan, H.
460 H.; Jagadish, C. *Nano Letters* **2013,** 13, (3), 1016-1022.
461 38. Zheng, C. L.; Wong-Leung, J.; Gao, Q.; Tan, H. H.; Jagadish, C.; Etheridge, J.
462 *Nano Letters* **2013,** 13, (8), 3742-3748.
463 39. Armitage, R.; Tsubaki, K. *Nanotechnology* **2010,** 21, (19), 195202.
464 40. Durand, C.; Bougerol, C.; Carlin, J. F.; Rossbach, G.; Godel, F.; Eymery, J.;
465 Jouneau, P. H.; Mukhtarova, A.; Butté, R.; Grandjean, N. *Acs Photonics* **2014,** 1, (1),
466 38-46.
467 41. Qian, F.; Brewster, M.; Lim, S. K.; Ling, Y. C.; Greene, C.; Laboutin, O.;
468 Johnson, J. W.; Gradecak, S.; Cao, Y.; Li, Y. *Nano Letters* **2012,** 12, (6), 3344-3350.
469 42. Carlberg, P.; Graczyk, M.; Sarwe, E. L.; Maximov, I.; Beck, M.; Montelius, L.
470 *Microelectron Eng* **2003,** 67-68, 203-207.

471 43. Eriksson, T.; Yamada, S.; Krishnan, P. V.; Ramasamy, S.; Heidari, B.
472 *Microelectron Eng* **2011,** 88, (3), 293-299.
473 44. Berg, A.; Lenrick, F.; Vainorius, N.; Beech, J. P.; Wallenberg, L. R.; Borgström,
474 M. T. *Nanotechnology* **2015,** 26, (43), 435601.
475 45. Borgström, M. T.; Wallentin, J.; Trägårdh, J.; Ramvall, P.; Ek, M.; Wallenberg,
476 L.; Samuelson, L.; Deppert, K. *Nano Research* **2010,** 3, (4), 264-270.
477 46. Berg, A.; Lehmann, S.; Vainorius, N.; Gustafsson, A.; Pistol, M.-E.;
478 Wallenberg, L. R.; Samuelson, L.; Borgström, M. T. *Journal of Crystal Growth* **2014,**
479 386, (0), 47-51.
480 47. Jacobsson, D.; Persson, J. M.; Kriegner, D.; Etzelstorfer, T.; Wallentin, J.;
481 Wagner, J. B.; Stangl, J.; Samuelson, L.; Deppert, K.; Borgström, M. T.
482 *Nanotechnology* **2012,** 23, (24), 245601.
483 48. Assali, S.; Zardo, I.; Plissard, S.; Kriegner, D.; Verheijen, M. A.; Bauer, G.;
484 Meijerink, A.; Belabbes, A.; Bechstedt, F.; Haverkort, J. E. M.; Bakkers, E. P. A. M.
485 *Nano Letters* **2013,** 13, (4), 1559-1563.
486 49. Green, T. A. *Gold Bull* **2014,** 47, (3), 205-216.
487 50. Heurlin, M.; Hultin, O.; Storm, K.; Lindgren, D.; Borgström, M. T.; Samuelson,
488 L. *Nano Letters* **2014,** 14, (2), 749-753.
489 51. Yazdi, S.; Berg, A.; Borgström, M. T.; Kasama, T.; Beleggia, M.; Samuelson,
490 L.; Wagner, J. B. *Small* **2015,** 11, (22), 2687-2695.
491 52. Nowzari, A.; Heurlin, M.; Jain, V.; Storm, K.; Hosseinnia, A.; Anttu, N.;
492 Borgström, M. T.; Pettersson, H.; Samuelson, L. *Nano Letters* **2015,** 15, (3), 1809-1814.
493 53. Lee, S. H.; Fetzer, C. M.; Stringfellow, G. B.; Choi, C. J.; Seong, T. Y. *Journal*
494 *of Applied Physics* **1999,** 86, (4), 1982-1987.
495 54. Wu, M. C.; Su, Y. K.; Chang, C. Y.; Cheng, K. Y. *Journal of Applied Physics*
496 **1985,** 58, (11), 4317-4321.
497 55. Clawson, A. R.; Hanson, C. M. *J Electron Mater* **1991,** 20, (5), 365-372.
498 56. Hou, X. Y.; Cai, W. Z.; He, Z. Q.; Hao, P. H.; Li, Z. S.; Ding, X. M.; Wang, X.
499 *Applied Physics Letters* **1992,** 60, (18), 2252-2254.
500 57. Ohno, T. *Phys Rev B* **1991,** 44, (12), 6306-6311.
501 58. Tian, S. S.; Wei, Z. P.; Li, Y. F.; Zhao, H. F.; Fang, X.; Tang, J. L.; Fang, D.;
502 Sun, L. J.; Liu, G. J.; Yao, B.; Ma, X. H. *Mat Sci Semicon Proc* **2014,** 17, 33-37.
503 59. Sköld, N.; Wagner, J. B.; Karlsson, G.; Hernan, T.; Seifert, W.; Pistol, M. E.;
504 Samuelson, L. *Nano Letters* **2006,** 6, (12), 2743-2747.
505 60. Wagner, J. B.; Sköld, N.; Wallenberg, L. R.; Samuelson, L. *Journal of Crystal*
506 *Growth* **2010,** 312, (10), 1755-1760.
507 61. Rudolph, D.; Funk, S.; Doblinger, M.; Morkötter, S.; Hertenberger, S.;
508 Schweickert, L.; Becker, J.; Matich, S.; Bichler, M.; Spirkoska, D.; Zardo, I.; Finley, J.
509 J.; Abstreiter, G.; Koblmüler, G. *Nano Letters* **2013,** 13, (4), 1522-1527.
510 62. Jiang, N.; Gao, Q.; Parkinson, P.; Wong-Leung, J.; Mokkapati, S.; Breuer, S.;
511 Tan, H. H.; Zheng, C. L.; Etheridge, J.; Jagadish, C. *Nano Letters* **2013,** 13, (11), 5135-
512 5140.
513 63. Zhang, Y.; Sanchez, A. M.; Wu, J.; Aagesen, M.; Holm, J. V.; Beanland, R.;
514 Ward, T.; Liu, H. *Nano Letters* **2015,** 15, (5), 3128-3133.
515 64. Meney, A. T.; Prins, A. D.; Phillips, A. F.; Sly, J. L.; Oreilly, E. P.; Dunstan, D.
516 J.; Adams, A. R.; Valster, A. *Ieee J Sel Top Quant* **1995,** 1, (2), 697-706.
517 65. Yow, H. K.; Houston, P. A.; Hopkinson, M. *Applied Physics Letters* **1995,** 66,
518 (21), 2852-2854.

519 66. Zhang, X. H.; Chua, S. J.; Fan, W. J. *Applied Physics Letters* **1998,** 73, (8),
520 1098-1100.

521
522
523 **Table of Contents Graphic**

524

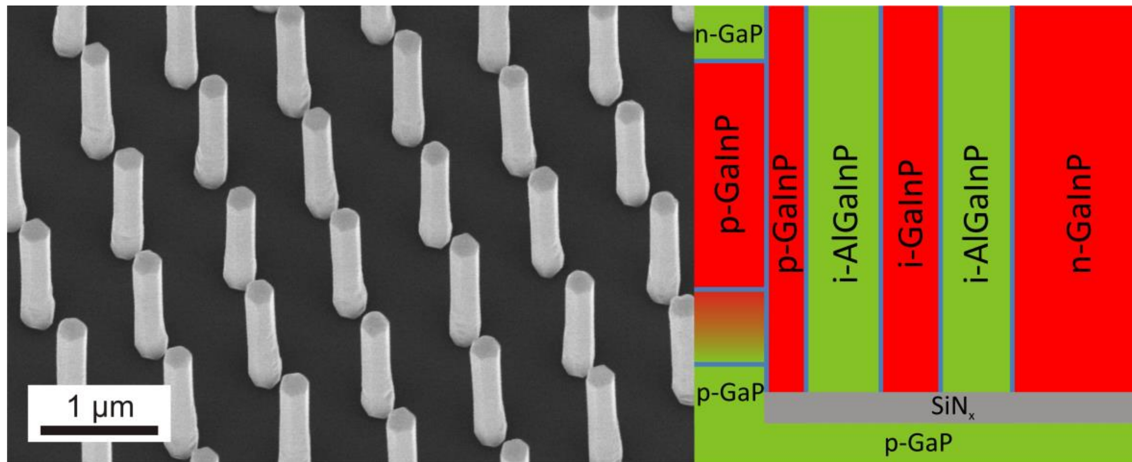

525